# Direct Hydroxide Attack Is a Plausible Mechanism for Amidase Antibody 43C9

LILLIAN T. CHONG, PRADIPTA BANDYOPADHYAY, THOMAS S. SCANLAN, IRWIN D. KUNTZ, PETER A. KOLLMAN[†]

*Graduate Group in Biophysics and Department of Pharmaceutical Chemistry, University of California, San Francisco, 600 16th Street, San Francisco, California 94143-2240*

*Received 29 October 2002; Accepted 24 February 2003*

**Abstract:** Direct hydroxide attack on the scissile carbonyl of the substrate has been suggested as a likely mechanism for esterase antibodies elicited by phosphonate haptens, which mimic the transition states for the alkaline hydrolysis of esters.[1] The unique amidase activity of esterase antibody 43C9 has been attributed to nucleophilic attack by an active-site histidine residue.[2] Yet, the active site of 43C9 is strikingly similar to those of other esterase antibodies, particularly 17E8. We have carried out quantum mechanical calculations, molecular dynamics simulations, and free energy calculations to assess the mechanism involving direct hydroxide attack for 43C9. Results support this mechanism and suggest that the mechanism is plausible for other antiphosphonate antibodies that catalyze the hydrolysis of (*p*-nitro)phenyl esters.

 J Comput Chem 24: 1371–1377, 2003

**Key words:** catalytic antibodies; amide/ester hydrolysis; quantum mechanical calculations; free energy calculations; molecular dynamics simulations

## Introduction

Catalytic antibody 43C9 is unique in its ability to cleave anilides. This antibody, which also hydrolyzes aryl esters, was elicited by an arylphosphamidate hapten (or transition-state analog). The crystal structure of 43C9 in complex with its ester hydrolysis product, *p*-nitrophenol, was recently solved.[3] Although the crystal structure of the hapten complex of 43C9 is unavailable, superposition of the *p*-nitrophenyl leaving group of the hapten onto the bound product and replacement of two crystallographic water molecules with the phosphonamidate oxygens (see Fig. 1) reveals a similar pattern of residues involved in hapten recognition as several other esterase antibodies—CNJ206, 48G7, and 17E8—that were elicited by arylphosphonate haptens and have crystal structures of their hapten-bound forms available.[1] This common motif consists of a deep hydrophobic pocket for the aryl leaving group and several hydrogen bond donating residues that stabilize the phosphamidate or phosphonate moiety of the hapten. Phosphonates and phosphamidates mimic the transition states involved in the base-promoted hydrolysis of esters and amides, respectively. Direct hydroxide attack, as programmed by the hapten, is therefore generally believed to be operative for the above esterase antibodies.[1]

A more sophisticated mechanism has been proposed for 43C9. Based on biochemical evidence, catalysis by 43C9 is suggested to involve the formation of a covalent acyl-antibody intermediate by nucleophilic attack of the substrate by an active-site histidine residue, His L91 (L = light chain), with subsequent deacylation by hydroxide ion (see Fig. 2A).[2,4] The role of His L91 as a nucleophile was suggested by the effects of mutating the residue to Gln in which a >50-fold decrease in catalytic efficiency resulted with little effect on ligand binding for the ester hydrolysis reaction.[5] This result is also consistent with a general base role for His L91 in which it may abstract a proton from water to form hydroxide ion. Histidine nucleophilic attack is also supported by detection of the acyl intermediate by electrospray mass spectrometry at pH 5.9 and its absence under the same conditions with the His L91→ Gln mutant.[6]

***Correspondence to:*** L. T. Chong; e-mail: ltchong@stanford.edu

[†]Peter A. Kollman passed away on May 25, 2001.

Contract/grant sponsors: NSF and a Burroughs-Wellcome Fellowships (to L.T.C.)

Contract/grant sponsor: NIH (to P.A.K.); contract/grant number: GM29072

This article includes Supplementary Material available from the authors upon request or via the Internet at ftp://ftp.wiley.com/public/journals/jcc/suppmat/24/1371 or http://www.interscience.wiley.com/jpages/0192-8651/suppmat/24/v24.1371.html

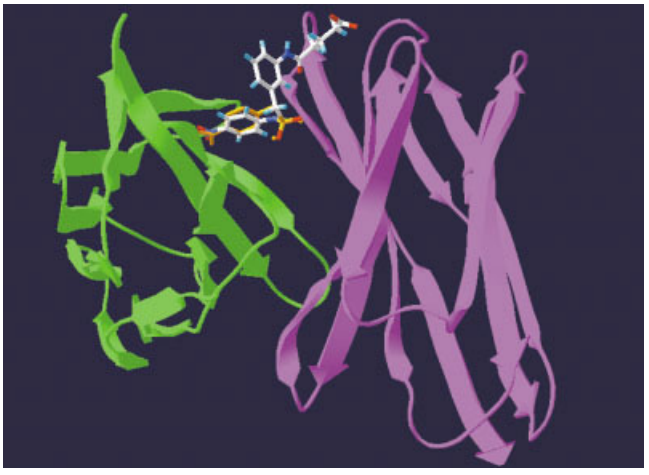

**Figure 1.** A model of antibody 43C9 in complex with its arylphosphamidate hapten. The crystal structure of the variable region of the antibody in complex with the ester hydrolysis product, *p*-nitrophenol, was used as a starting point for building the model.[3] The active site lies in a cleft between the light (green) and heavy (magenta) chains of the antibody. As done by Thayer et al.,[3] the hapten was docked into the active site by superposition of the *p*-nitrophenyl leaving group of the hapten onto the bound product (orange) and replacement of two crystallographic water molecules (shown as orange spheres) with the phosphonamidate oxygens. Produced using Swiss-Pdb Viewer.[47]

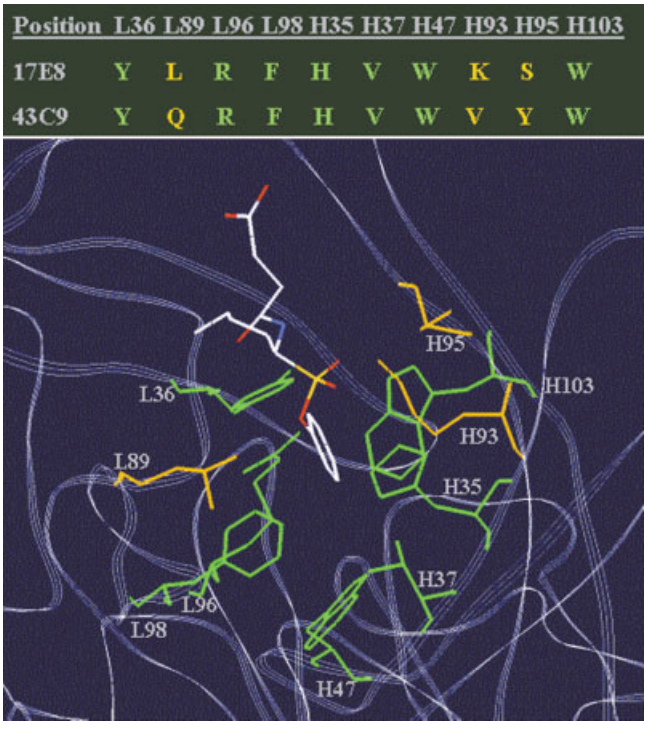


**Figure 3.** Active site residues of 17E8 that contact the arylphosphonate moiety of its hapten.[13] Seven out of these ten residues are identical in 43C9 as shown above in green both in the snapshot of the active site (produced by Swiss-Pdb Viewer[47]) and in the sequence analysis taken from MacBeath and Hilvert.[1] Residues that differ from those in 43C9 are shown in orange.

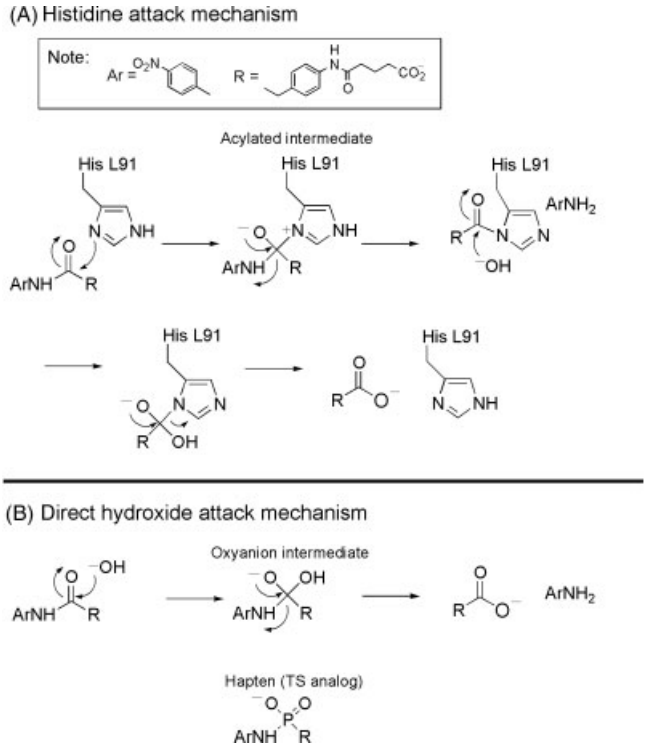


**Figure 2.** Proposed mechanisms of catalysis by 43C9, which hydrolyzes the anilide substrate shown above as well as the corresponding aryl ester substrate: (A) nucleophilic attack by His L91 (as proposed by Benkovic et al.[2] ) and (B) direct hydroxide attack as programmed by the hapten. The hydroxide ion in (B) is likely produced by abstraction of a proton from water by His L91. These mechanisms were also predicted to apply to the aryl ester substrate.

It is surprising that 43C9 should have a mechanism that is so different from that programmed by its hapten (see Fig. 2B), particularly given that the active site of 43C9 has striking similarities to that of esterase antibody 17E8, which most likely functions via direct hydroxide attack.[1] Based on sequence analysis, 7 out of 10 residues in the vicinity of the arylphosphonate moiety of the hapten in 17E8 are identical in 43C9 (see Fig. 3).[1] Here we explore the plausibility of direct hydroxide attack as a mechanism of catalysis for 43C9 relative to 17E8 through quantum mechanical (QM) calculations, molecular dynamics (MD) simulations, and MM-PBSA free energy calculations.[7]

## Methods

### *QM Calculations*

*p*-Nitrophenyl acetate and *p*-nitroacetanilide were used as minimal representations of the *p*-nitrophenyl ester and *p*-nitroanilide substrates of 43C9, respectively. Likewise, phenyl acetate and acetanilide were used to represent the phenyl ester and amide substrates of 17E8, respectively. Reported energies for stationary points along the reaction path are from calculations carried out at

the B3LYP/6-31+G*//B3LYP/6-31+G* level with zero point energy corrections (scaled by 0.9806)[8] derived from frequency calculations at the corresponding level. Stationary points were characterized by calculating the Hessian matrix of energy second derivatives and by determining the number of imaginary frequencies. Intrinsic reaction coordinate (IRC) calculations were used to confirm the minima connected by each saddle point. Optimized geometries of reactants and transition states at the B3LYP/6-31+G* level are provided in the Supplemental Material. Conductor-like screening model (COSMO)[9] self-consistent reaction field (SCRF) single-point calculations at the B3LYP/6-31+G* level were performed at selected stationary points to estimate environmental effects. A dielectric constant value of 78.4 was used to simulate an aqueous environment, while a value of 4, which accounts for the response of the dipolar groups of the polypeptide backbone,[10] was used to approximate the protein environment. Geometries in which the hydroxide ion was positioned near the amide hydrogen of *p*-nitroacetanilide led to deprotonation to form a water molecule and an ionized substrate that was inert to hydrolysis. This side reaction was avoided in an optimized geometry where the hydroxide ion was positioned ~1 Å further away from the amide hydrogen. All *ab initio* calculations were performed with the GAUSSIAN 98 program.[11]

### *MD Simulation Protocol*

Models of each complex were prepared using the LeAP module of the AMBER 5.0 package.[12] The crystal structure of the single-chain variable fragment of 43C9 in complex with the *p*-nitrophenol ester hydrolysis product (43CA in the Protein Data Bank)[3] was used as a starting point for building a model of the 43C9-hapten complex. As done by Thayer et al.,[3] superposition of the hapten's *p*-nitrophenyl group onto the bound *p*-nitrophenol and rotation about the C-N-P-C bond positions the hapten's two phosphamidate oxygen atoms close to the crystallographic waters 481 and 584. All crystallographic waters except for waters 481 and 584 were included in the starting model. Coordinates for the 17E8-hapten complex were taken from the 2.5-Å resolution crystal structure of the antibody binding fragment of 17E8 in complex with its hapten (1EAP in the Protein Data Bank).[13] No crystallographic waters were present in this crystal structure. Because the variable region of each antibody is sufficient for full antibody activity,[14] only the first 113 residues of the light chain (L) and the first 117 residues of the heavy chain (H) were included to represent the antibody. *N*-methyl capping groups were added to the C-terminal truncated ends while the N-terminal ends were treated as charged. Ionization states present in neutral solution were used for all charged residues. Tautomeric states of histidine residues (HID = protonation at the δ-nitrogen, HIE = protonation at the ε-nitrogen) were determined by analysis of hydrogen bonds; in ambiguous cases, the residues were assigned to be HIE, which is the predominant tautomer for free histidines in solution.[15] Both His H35 and His L91 were assigned to be HIE for the ground-state (GS) complexes of 43C9 and HID in the transition-state (TS) complexes. In the TS complexes of 17E8, His L38, His L49, His H32, and His H35 were assigned to be HID, HIE, HID, and HIE, respectively; the same tautomeric forms were used for the GS complexes except that His H35 was assigned to be HID.

Models for GS and TS complexes were obtained by starting with the antibody–hapten complex structures, then using the haptens as scaffolds to build the GS and TS ligands. TS ligands were approximated by tetrahedral intermediates (shown in Fig. 2). To be consistent with the Cornell et al. force field,[16] charges for all ligands were determined by the restrained electrostatic potential (RESP) fitting method,[17] using electrostatic potentials that were derived from HF/6-31G*//HF/6-31G* quantum mechanical calculations. Quantum mechanical calculations were performed using the Gaussian 98 package.[11] Because geometry optimization of the tetrahedral, hydrolysis intermediate for the *p*-nitrophenyl ester substrate of 43C9 yielded the products, an optimization was performed while constraining the scissile ester bond to the length (1.53 Å) of the corresponding bond in the optimized geometry of the hydrolysis intermediate for the phenyl ester substrate of 17E8. All ligand parameters not present in the Parm99 parameter set[18] are reported in the Supplementary Material.

In each MD simulation, we concentrated our attention on the binding site region of the antibody, permitting only residues (including ions, water molecules, and the ligand) that lie within 18 Å of the Cζ atom of Arg L96 to move. This mobile set of residues will be referred to as the "belly" region. Each antibody-ligand complex was solvated by placing a sphere of TIP3P water molecules[19] with a radius of 31 Å centered at the Cζ atom of Arg L96 and then simulated using an identical protocol and the AMBER 5.0 suite of programs.[12] To fix any errors introduced in the model-building process, the molecular mechanics model described above was first subjected to 100 steps of steepest descent minimization followed by 1000 steps of conjugate gradient minimization. After this minimization, the system was equilibrated in two stages. At the beginning of each stage, the temperature is raised from 0 to 300 K during the first 2 ps, after which the temperature remained at 300 K. In the first stage, only the ligand, ions in the belly region, and all waters were equilibrated for 40 ps. In the second stage, the entire belly region was equilibrated for 60 ps. Sampling of reasonable configurations for the resulting stable state of the antibody–ligand structure was obtained by running a 600-ps belly simulation with a 2-fs time step at 300 K. For each simulation, Berendsen temperature coupling[20] was used to maintain the system at its assigned temperature, while the SHAKE algorithm constrained the length of all bonds to their equilibrium values.[21] To minimize computational expense, long-ranged nonbonded interactions were only calculated out to a 12-Å residue-based cutoff distance. To allow for sufficient equilibration, only the latter 500 ps of each 600-ps simulation were used for subsequent analysis of the dynamics.

### *MM-PBSA Protocol*

To compute the average binding free energy of each antibody–ligand complex, we selected 50 equally spaced "snapshot" configurations of the unbound antibody, unbound ligand, and antibody–ligand complex from the 101–600-ps interval of the 600-ps complex trajectory and performed energy calculations on the snapshots. Prior to the energy calculations, all waters and ions were removed from each snapshots. Free energy calculations were performed using the MM-PBSA approach, described in detail by

**Table 1.** Computed Barriers (kcal/mol) at the B3LYP/6-31+G*//B3LYP/6-31+G* Level for Ester and Amide Hydrolysis Reactions of 43C9 and 17E8 via Hydroxide Attack with Rate-Limiting Barriers Underlined.

| | | | $\varepsilon = 1$ | $\varepsilon = 4$ | $\varepsilon = 78.4$ |
|---|---|---|---|---|---|
| 43C9 | ester hydrolysis | TS1 | 2.0 | 4.4 | 18.7 |
| | amide hydrolysis | TS1 | 6.1 | 7.1 | 19.3 |
| | | TS2 | −12.7 | −3.3 | 13.5 |
| 17E8 | ester hydrolysis | TS1 | 2.8 | 9.5 | 18.4 |
| | amide hydrolysis | TS1 | 7.8 | 15.9 | 25.9 |
| | | TS2 | −1.0 | 20.9 | 37.0 |

As described in Methods, minimal representations of the ester and amide substrates were used in the calculations. Gas-phase values include zero-point corrections. The COSMO continuum model was used with dielectric constant ($\varepsilon$) values of 4 and 78.4. Only one transition state involving hydroxide addition (TS1) was located for each of the ester hydrolysis reactions while a second transition state involving breakdown of the intermediate (TS2) was located for each of the amide hydrolysis reactions.

Srinivasan et al.[7] The binding free energy, $\Delta G_{\text{bind}}$, is defined as follows:

$$\Delta G_{\text{bind}} = \Delta E_{\text{MM}} + \Delta G_{\text{solv}} - T\Delta S$$

$$\Delta E_{\text{MM}} = \Delta E_{\text{es}} + \Delta E_{\text{vdW}} + \Delta E_{\text{int}}$$

$$\Delta G_{\text{solv}} = \Delta G_{\text{PB}} + \Delta G_{\text{SA}}$$

where $\Delta E_{\text{MM}}$ is the change in the total MM energy of the solute with an electrostatic component ($\Delta E_{\text{es}}$), a van der Waals component ($\Delta E_{\text{vdW}}$), and an internal component ($\Delta E_{\text{int}}$) consisting of bond, angle, and torsional energies; $\Delta G_{\text{solv}}$ is the solvation energy difference, which consists of an electrostatic contribution ($\Delta G_{\text{PB}}$) determined by the Poisson–Boltzmann approach using the DelPhi2.0 software package[22] and a nonelectrostatic contribution ($\Delta G_{\text{SA}}$) that is linearly dependent on the solvent accessible surface area [$\Delta G_{\text{SA}} = \gamma\,(\Delta\text{SASA}) + \beta$ where $\gamma = 0.00542$ and $\beta = 0.92$ kcal/mol ]; and $-T\Delta S$ is the solute entropic contribution to the binding free energy. Solute entropic contributions were not calculated in this study since they are only crudely estimated by normal-mode analysis and likely to be similar for all the antibody–ligand complexes. To estimate the absolute binding free energies, a value of +20 kcal/mol was used, based on published results for the 48G7-hapten complex.[23] Because the same antibody and ligand configurations are used for their respective unbound and bound states, $\Delta E_{\text{int}}$ is equal to zero. Calculations of the electrostatic component to the MM energy and the electrostatic contribution to the solvation energy were performed using a solute, or "interior," dielectric ($\varepsilon_{\text{int}}$) value of 1, consistent with our use of a nonpolarizable molecular mechanics force field. In this free energy approach, the solute response to charge fluctuations is estimated through explicit averaging of conformations taken from an MD simulation rather than using an interior dielectric constant that is greater than unity for a single, static conformation.

## Results and Discussion

The majority of the previous QM studies on the base-promoted hydrolysis of esters or amides have focused on alkyl esters such as methyl acetate,[24–28] methyl benzoate,[26,27] methyl formate,[29] and cocaine;[30,31] and on the alkyl amide, formamide.[32–36] Only two studies have examined hydroxide addition to aryl esters, which are activated esters that are easier to hydrolyze than alkyl esters. Luzhov and Venanzi reported AM1 calculations for hydroxide addition to phenyl acetate in the gas phase and in solution.[37] In a study on the fidelity of phosphonate haptens, Tantillo and Houk performed detailed analyses of the complete reaction pathways for hydroxide attack on phenyl acetate and on *p*-nitrophenyl acetate at the HF/6-31+G*//HF/6-31+G* and MP2/6-31+G*//HF/6-31+G* levels in the gas phase; incorporating solvation effects through PCM and SCI-PCM calculations.[38] Hydroxide addition to anilides has not been examined. Here, we have extended the work of Tantillo and Houk[39] to the analyses of hydroxide attack on phenyl acetate, *p*-nitrophenyl acetate, and on the corresponding anilides at the B3LYP/6-31+G*//B3LYP/6-31+G* level with incorporation of solvent effects through the COSMO continuum model.[9]

As discussed in the Introduction, His L91 of 43C9 is likely to act as a general base, abstracting a proton from water to form hydroxide ion. Likewise, the catalytic residue of 17E8, His H35, may act as a general base to produce hydroxide ion. Table 1 shows the computed barriers for hydroxide attack on *p*-nitrophenyl acetate and *p*-nitroacetanilide, which are minimal representations of the ester and amide substrates for 43C9, respectively; and on phenyl acetate and acetanilide, which represent the ester and amide substrates of 17E8, respectively. The ester hydrolysis reactions were each concerted with the location of only one transition state (TS1) while the amide hydrolysis reactions were each stepwise, involving both an addition transition state (TS1) and an elimination transition state (TS2). In the gas-phase ($\varepsilon = 1$), the activation barrier for the 43C9 amide hydrolysis reaction is ~4 kcal/mol greater than that for the corresponding ester hydrolysis reaction, consistent with the experimental difference of ~6 kcal/mol.[40,41] The ~5 kcal/mol greater activation barrier for the 17E8 amide hydrolysis reaction relative to the corresponding ester hydrolysis reaction is not as great as might be expected because amidase activity by 17E8 is undetectable. However, incorporation of environmental effects by using the COSMO continuum model[9] with

dielectric constants of 4 and 78.4 dramatically increases this difference to ~11 kcal/mol and ~19 kcal/mol, respectively. These differences are much greater than those found for the hydrolysis reactions of 43C9. The greater differences might be explained by the fact that aniline is a much poorer leaving group than *p*-nitrophenyl aniline due to the absence of the electron-withdrawing nitro group (the $pK_a$ values of aniline and *p*-nitroaniline are 27 and 18.5, respectively) while the leaving group abilities of phenol and *p*-nitrophenol are more similar ($pK_a$ values of 10 and 7, respectively). Interestingly, the rate-limiting step for the amide hydrolysis reaction changes from hydroxide addition to breakdown of the intermediate when dielectric constants of 4 and 78.4 were used. As shown in Figure 4, computed barriers for the hydrolysis reactions of both 43C9 and 17E8 increase with the polarizability of the environment into the range of experiment.

To estimate the ground-state (GS) and transition-state (TS) stabilizations of each hydrolysis reaction, we computed the binding free energies for the GS and TS complexes using the MM-PBSA free energy approach,[7] which uses a hybrid of molecular mechanics and continuum solvent models. This approach has given accurate relative binding free energies in a number of studies.[42] A model of each GS or TS complex was constructed by modifying the hapten in the hapten complex to the substrate or tetrahedral intermediate, respectively. Hydroxide ion was not included in the GS complexes because the ion is likely present at only catalytic and not stoichiometric amounts during the catalyzed reaction. Tetrahedral intermediates were used to approximate transition states due to their similar geometries and charge distributions. The intermediate resulting from *re* attack by hydroxide ion was energetically preferred by 43C9 while the *si* enantiomer was preferred by 17E8, consistent with findings by Tantillo and Houk.[39] As shown in Table 2, both the computed GS and TS stabilizations are similar for the ester and amide hydrolysis reactions of 43C9 with a 1 kcal/mol greater GS stabilization and a 1.2 kcal/mol greater TS stabilization for the amide hydrolysis reaction relative to the ester hydrolysis reaction. These results agree with estimated values from kinetic data where the GS stabilizations for the ester and amide hydrolysis reactions of 43C9 are within 1 kcal/mol of each other as are the transition-state stabilizations.[40,41] Computed GS and TS stabilizations are also similar for the ester and amide hydrolysis reactions of 17E8 with a 0.5 kcal/mol less GS stabilization and 0.9 kcal/mol less TS stabilization for the amide hydrolysis reaction relative to the ester hydrolysis reaction (see Table 2). Because no kinetic parameters were measurable for the amide hydrolysis reaction of 17E8, there is no experimental validation for the latter computed results. Nonetheless, for the ester hydrolysis reaction of 17E8, the computed relative stabilizations of the transition state to the ground state of −6.1 kcal/mol is in good agreement with the estimated experimental value of −5.3 kcal/mol.[43]

Dynamics of the GS complexes in our MD simulations of the complexes suggest that direct hydroxide attack is plausible for 43C9. In each GS complex simulation for 43C9, one or two water molecules are found within 4 Å of the substrate carbonyl carbon in 41% of the 500 configurations sampled per ps from each simulation. Interestingly, the dynamics are also consistent with nucleophilic attack by His L91 with the distance between the nucleophilic nitrogen of His L91 (protonated at the ε–nitrogen) and the carbonyl carbon of the substrate ranging between 3.7 to 5.5 Å.

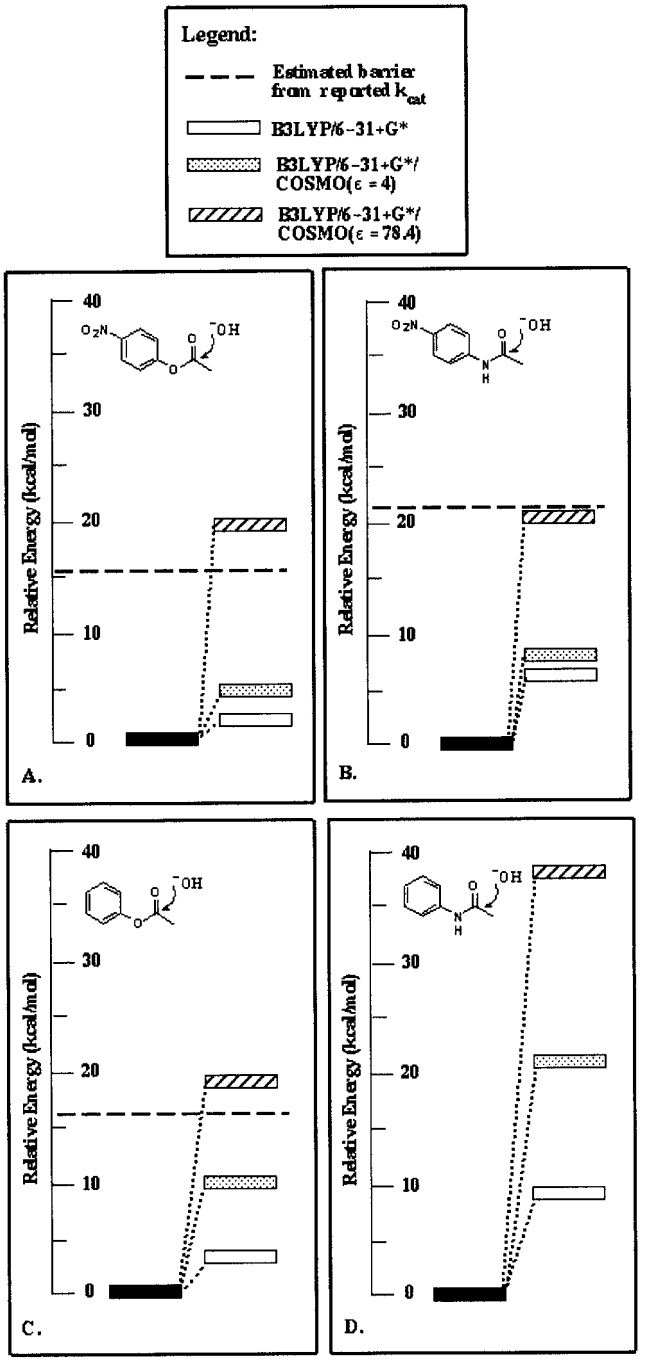


**Figure 4.** Computed activation barriers of hydrolysis via hydroxide attack on *p*-nitrophenyl acetate (A) and *p*-nitroacetanilide (B), which are minimal representations of the ester and amide substrates of 43C9, respectively. Also shown are computed barriers of hydrolysis for phenyl acetate (C) and acetanilide (D), which are minimal representations of the ester and amide substrates of 17E8, respectively. Experimental barriers for the 43C9 ester and amide hydrolysis reactions were estimated from $k_{cat}$ values of 1500 $min^{-1}$ (15.5 kcal/mol) and 0.08 $min^{-1}$ (21.4 kcal/mol), respectively.[40,41] The experimental barrier for the 17E8 ester hydrolysis reaction was estimated from the $k_{cat}$ value of 223 $min^{-1}$ (16.7).[48] No experimental barrier for the reaction in (D) is shown because amidase activity was not detectable for 17E8.

**Table 2.** Computed Average Binding Energies (kcal/mol) for Ground-State (GS) and Transition-State (TS) Complexes of 43C9 and 17E8 with Standard Errors of the Mean in Parentheses.

| | | GS Complex | | TS Complex | |
|---|---|---|---|---|---|
| | | Computed | Experiment | Computed | Experiment |
| 43C9 | ester hydrolysis | 4.3 (0.6) | −5.8[a] | −1.0 (0.8) | −11.9[a] |
| | amide hydrolysis | 3.3 (0.4) | −4.4[a] | −2.2 (0.6) | −11.7[a] |
| 17E8 | ester hydrolysis | 1.4 (0.5) | −4.6[b] | −5.2 (0.5) | −9.9[b] |
| | amide hydrolysis | 1.9 (0.5) | — | −4.3 (0.6) | — |

Fifty equally spaced configurations from the 101–600-ps intervals of the MD simulations were used for the computations. TS ligands were approximated by the energetically preferred enantiomers (*re* for the 43C9 ligand and *si* for the 17E8 ligand) of the tetrahedral intermediates resulting from hydroxide attack. As mentioned in Methods, the solute entropic contribution for each complex was not computed, but approximated to be +20 kcal/mol[23] to obtain an estimate of the absolute binding free energy.

[a]Estimated from kinetic data on 43C9.[40,41]

[b]Estimated from kinetic data on 17E8 (no detectable amidase activity).[43]

The possibility of histidine attack by 43C9 cannot be ruled out given the detection of the acyl-antibody intermediate by mass spectrometry. Nonetheless, our results suggest that this more complex mechanism, which could not result directly from hapten recognition, provides no catalytic advantage over the more simple hydroxide attack mechanism that would result directly from hapten recognition. Both mechanisms may indeed be operative. Detailed mechanistic inferences should be tentative for 43C9 at this time because a high-resolution structure of the 43C9–hapten complex is not available. Furthermore, our results are only semiquantitative due to the use of a continuum model to incorporate environmental effects on the activation barriers in the QM calculations. More accurate computations of the barriers would involve explicit incorporation of the protein environment as has been done in various hybrid QM and molecular mechanics approaches.[44,45] Given the large computational demands of such approaches, convergence problems that often emerge from their use, and the uncertainty of the 43C9–hapten complex model, these approaches were not applied in this study.[46]

## Conclusions

Our results support the proposed mechanism of catalysis by 43C9 in which the active-site residue, His L91, abstracts a proton from a nearby water to form hydroxide ion, which then attacks the aryl ester or anilide substrate. Computed activation barriers are in range of experimental values while the dynamics of the GS complexes support the plausibility of direct hydroxide attack. Finally, free energy calculations predict that the GS and TS stabilizations are similar for the ester and amide hydrolysis reactions of 43C9, which is consistent with experiment. The proposed mechanism might be generalized to all antibodies that have been elicited by arylphosphonate or arylphosphamidate haptens.

## Acknowledgments

The authors thank K. Houk and D. Tantillo for helpful suggestions on improving the manuscript.

## References

1. MacBeath, G.; Hilvert, D. Chem Biol 1996, 3, 433.
2. Benkovic, S. J.; Adams, J. A.; Borders, C. L., Jr.; Janda, K. D.; Lerner, R. A. Science 1990, 250, 1135.
3. Thayer, M. M.; Olender, E. H.; Arvai, A. S.; Koike, C. K.; Canestrelli, I. L.; Stewart, J. D.; Benkovic, S. J.; Getzoff, E. D.; Roberts, V. A. J Mol Biol 1999, 291, 329.
4. Stewart, J. D.; Krebs, J. F.; Siuzdak, G.; Berdis, A. J.; Smithrud, D. B.; Benkovic, S. J. Proc Natl Acad Sci USA 1994, 91, 7404.
5. Stewart, J. D.; Roberts, V. A.; Thomas, N. R.; Getzoff, E. D.; Benkovic, S. J. Biochemistry 1994, 33, 1994.
6. Krebs, J. F.; Siuzdak, G.; Dyson, H. J.; Stewart, J. D.; Benkovic, S. J. Biochemistry 1995, 34, 720.
7. Srinivasan, J.; Miller, J.; Kollman, P. A.; Case, D. A. J Biomol Struct Dyn 1998, 16, 671.
8. Scott, A. P.; Radom, L. J. Phys Chem 1996, 100, 16502.
9. Barone, V.; Cossi, M.; Tomasi, J. J Comput Chem 1998, 19, 404.
10. Gilson, M.; Honig, B. Biopolymers 1986, 25, 2097.
11. Frisch, M. J.; Trucks, G. W.; Schlegel, H. B.; Scuseria, G. E.; Robb, M. A.; Cheeseman, J. R.; Zakrzewski, V. G.; Montgomery, J. A., Jr.; Stratmann, R. E.; Burant, J. C.; Dapprich, S.; Millam, J. M.; Daniels, A. D.; Kudin, K. N.; Strain, M. C.; Farkas, O.; Tomasi, J.; Barone, V.; Cossi, M.; Cammi, R.; Mennucci, B.; Pomelli, C.; Adamo, C.; Clifford, S.; Ochterski, J.; Petersson, G. A.; Ayala, P. Y.; Cui, Q.; Morokuma, K.; Malick, D. K.; Rabuck, A. D.; Raghavachari, K.; Foresman, J. B.; Cioslowski, J.; Ortiz, J. V.; Stefanov, B. B.; Liu, G.; Liashenko, A.; Piskorz, P.; Komaromi, L.; Gomperts, R.; Martin, R. L.; Fox, D. J.; Keith, T.; Al-Laham, M. A.; Peng, C. Y.; Nanayakkara, A.; Gonzalez, C.; Challacombe, M.; Gill, P. M. W.; Johnson, B. G.; Chen, W.; Wong, M. W.; Andres, J. L.; Head–Gordon, M.; Replogle, E. S.; Pople, J. A. Gaussian 98; Gaussian, Inc.: Pittsburgh, PA, 1998.
12. Case, D. A.; Pearlman, D. A.; Caldwell, J. W.; Cheatham, T. E., III; Ross, W. S.; Simmerling, C.; Darden, T.; Merz, K. M.; Stanton, R. V.; Cheng, A.; Vincent, J. J.; Crowley, M.; Ferguson, D. M.; Radmer, R.; Seibel, G. L.; Singh, U. C.; Weiner, P.; Kollman, P. A. Amber 5.0; University of California: San Francisco, CA, 1997.
13. Zhou, G. W.; Guo, J.; Huang, W.; Fletterick, R. J.; Scanlan, T. S. Science 1994, 265, 1059.
14. Gibbs, R. A.; Posner, B. A.; Filpula, D. R.; Dodd, S. W.; Finkelman, M. A.; Lee, T. K.; Wroble, M.; Whitlow, M.; Benkovic, S. J. Proc Natl Acad Sci USA 1991, 88, 4001.

15. Tanokura, M.; Tasumi, M.; Miyazawa, T. Biopolymers 1976, 15, 393.
16. Cornell, W. D.; Cieplak, P.; Bayly, C. I.; Gould, I. R.; Merz, K. M.; Ferguson, D. M.; Spellmeyer, D. C.; Fox, T.; Caldwell, J. W.; Kollman, P. A. J Am Chem Soc 1995, 117, 5179.
17. Bayly, C. I.; Cieplak, P.; Cornell, W. D.; Kollman, P. A. J Phys Chem 1993, 97, 10269.
18. Wang, J.; Cieplak, P.; Kollman, P. A. J Comput Chem 2000, 21, 1049.
19. Jorgensen, W.; Chandrasekhar, J.; Madura, J.; Impey, R.; Klein, M. J Chem Phys 1983, 79, 926.
20. Berendsen, H.; Postma, J.; van Gusteren, W.; DiNola, A.; Haak, J. J Comput Phys 1984, 81, 3684.
21. Ryckaert, J.; Ciccotti, G.; Berendsen, H. J Comput Phys 1977, 23, 327.
22. Sharp, K. A.; Honig, B. Annu Rev Biophys Biophys Chem 1990, 19, 301.
23. Chong, L. T.; Duan, Y.; Wang, L.; Massova, I.; Kollman, P. A. Proc Natl Acad Sci USA 1999, 96, 14330.
24. Ohkubo, K.; Urata, Y.; Seri, K.; Ishida, H.; Sagawa, T.; Nagashima, T.; Imagawa, Y. J Mol Catal 1994, 90, 355.
25. Teraishi, K.; Saito, M.; Fujii, I.; Nakamura, H. Tetrahedron Lett 1992, 33, 7153.
26. Sherer, E. C.; Turner, G. M.; Shields, G. C. Int J Quantum Chem Quantum Biol Symp 1995, 22, 83.
27. Turner, G. M.; Sherer, E. C.; Shields, G. C. Int J Quantum Chem Quantum Biol Symp 1995, 22, 103.
28. Hori, K. J Chem Soc Perkin Trans 1992, 1, 1629.
29. Pranata, J. J Phys Chem 1994, 98, 1180.
30. Sherer, E. C.; Turner, G. M.; Lively, T. N.; Landry, D. W.; Shields, G. C. J Mol Model 1996, 2, 62.
31. Sherer, E. C.; Yang, G.; Turner, G. M.; Shields, G. C.; Landry, D. W. J Phys Chem A 1997, 101, 8526.
32. Bakowies, D.; Kollman, P. A. J Am Chem Soc 1999, 121, 5712.
33. Madura, J. D.; Jorgensen, W. J Am Chem Soc 1986, 1986, 2517.
34. Alagona, G.; Scrocco, E.; Tomasi, J. J Am Chem Soc 1975, 97, 6976.
35. Krug, J. P.; Popelier, P. L. A.; Bader, R. F. W. J Phys Chem 1992, 96, 7604.
36. Weiner, S. J.; Singh, U. C.; Kollman, P. A. J Am Chem Soc 1985, 107, 2219.
37. Luzhkov, V. B.; Venanzi, C. A. J Phys Chem 1995, 99, 2312.
38. Tantillo, D. J.; Houk, K. N. J Org Chem 1999, 64, 3066.
39. Tantillo, D. J.; Houk, K. N. J Comput Chem 2002, 23, 84.
40. Gibbs, R. A.; Benkovic, P. A.; Janda, K. D.; Lerner, R. A.; Benkovic, S. J. J Am Chem Soc 1992, 114, 3528.
41. Janda, K. D.; Schloeder, D.; Benkovic, S. J.; Lerner, R. A. Science 1988, 241, 1188.
42. Kollman, P. A.; Massova, I.; Reyes, C.; Kuhn, B.; Huo, S.; Chong, L.; Lee, M.; Lee, T.; Duan, Y.; Wang, W.; Donini, O.; Cieplak, P.; Srinivasan, J.; Case, D. A.; Cheatham, T. E., 3rd Acc Chem Res 2000, 33, 889.
43. Guo, J. C.; Huang, W.; Scanlan, T. S. J Am Chem Soc 1994, 116, 6062.
44. Kollman, P. A.; Kuhn, B.; Donini, O.; Perakyla, M.; Stanton, R.; Bakowies, D. Acc Chem Res 2001, 34, 72.
45. Warshel, A. Computer Modeling of Chemical Reactions in Enzymes and Solutions; Wiley: New York, 1991.
46. Lee, T. S.; Chong, L. T.; Chodera, J. D.; Kollman, P. A. J Am Chem Soc 2001, 123, 12837.
47. Guex, N.; Peitsch, M. C. Electrophoresis 1997, 18, 2714.
48. Guo, J.; Huang, W.; Zhou, G. W.; Fletterick, R. J.; Scanlan, T. S. Proc Natl Acad Sci USA 1995, 92, 1694.